Available online at www.sciencedirect.com
SCIENCE DIRECT®
International Journal of Heat and Mass Transfer 48 (2005) 5602–5615
International Journal of HEAT and MASS TRANSFER
www.elsevier.com/locate/ijhmt

Saturated flow boiling heat transfer and associated bubble characteristics of R-134a in a narrow annular duct

Y.M. Lie, T.F. Lin *

Department of Mechanical Engineering, National Chiao Tung University, Hsinchu, Taiwan ROC

Received 13 March 2005; received in revised form 21 May 2005
Available online 4 October 2005

Abstract

Experiments are conducted here to investigate how the channel size affects the saturated flow boiling heat transfer and associated bubble characteristics of refrigerant R-134a in a horizontal narrow annular duct. The gap of the duct is fixed at 1.0 and 2.0 mm in this study. The measured heat transfer data indicate that the saturated flow boiling heat transfer coefficient increases with a decrease in the gap of the duct. Besides, raising the imposed heat flux can cause a significant increase in the boiling heat transfer coefficients. However, the effects of the refrigerant mass flux and saturated temperature on the boiling heat transfer coefficient are milder. The results from the flow visualization show that the mean diameter of the bubbles departing from the heating surface decreases slightly at increasing R-134a mass flux. Moreover, the bubble departure frequency increases at reducing duct size mainly due to the rising shear stress of the liquid flow, and at a high imposed heat flux many bubbles generated from the cavities in the heating surface tend to merge together to form big bubbles. Correlation for the present saturated flow boiling heat transfer data of R-134a in the narrow annular duct is proposed. Additionally, data for some quantitative bubble characteristics such as the mean bubble departure diameter and frequency and the active nucleation site density are also correlated.

1. Introduction

Due to the high thermal efficiency, small size, and energy saving, compact heat exchangers have been used widely in various technological applications involving phase changes of working fluids. Recently there has been a growing awareness of the benefits from process intensification and the reduction in plant size for a given capacity. This has led to a requirement for smaller evaporators [1,2], which in turn motivates the recent intensive studies on flow boiling in small channels [3–17]. Flow boiling characteristics of some fluids in single, small, circular and rectangular channels have received most attention [3–14]. Some other studies investigate boiling in a narrow concentric duct [15–17]. The results from these studies indicate that as the channel size is smaller than certain critical value, the two-phase flow regimes and the associated heat transfer differ significantly from those in channels of conventional size. Which heat transfer mechanism is dominant is the main issue of many investigations. In general, convection dominates for low values of heat flux and wall superheat and for high vapor qualities, while nucleate boiling dominates at the opposite conditions. A number of experimental studies have been conducted on flow boiling in small channels

* Corresponding author. Tel.: +886 35 712121 55118; fax: +886 35 726 6 440.
E-mail address: tflin@mail.nctu.edu.tw (T.F. Lin).

0017-9310/$ - see front matter © 2005 Elsevier Ltd. All rights reserved.
doi:10.1016/j.ijheatmasstransfer.2005.05.013

Nomenclature

A_{cs}	cross-sectional area of the annular duct, m^2
A_s	outside surface area of the heated inner pipe, m^2
Bo	Boiling number, $Bo = \frac{q}{G \cdot i_{fg}}$, dimensionless
c_{pr}	specific heat of the liquid refrigerant, J/kg °C
D_h	hydraulic diameter, m
d_P	mean bubble departure diameter, m
f	mean bubble departure frequency, Hz
f_f	friction factor for liquid flow
g	acceleration due to gravity, m/s^2
G	mass flux, kg/m^2 s
$h_{1\phi}$	single-phase liquid convection heat transfer coefficient, W/m^2 °C
h_r	saturated flow boiling heat transfer coefficient, W/m^2 °C
i_{fg}	enthalpy of vaporization, J/kg
I	measured electric current from DC power supply, A
k_l	thermal conductivity of liquid R-134a, W/m °C
N_{ac}	active nucleation site density, n/m^2
N_{conf}	confinement number, $N_{conf} = \frac{(\sigma/(g\Delta\rho))^{0.5}}{D_h}$, dimensionless
Nu	Nusselt number for single-phase liquid flow, $Nu = \frac{h_{1\phi} D_h}{k_l}$, dimensionless
P	system pressure, kpa
Pr_l	Prandtl number of liquid R-134a, dimensionless
q	average imposed heat flux, W/m^2
q_b, q_c, q_t	heat flux due to bubble nucleation, single-phase convection, total value, W/m^2
Q_n, Q_s	net and total power input, W
Re_l	all liquid Reynolds number, dimensionless
T_{sat}	saturated temperature of refrigerant R-134a, °C
T_w	wall temperature of heated inner pipe, °C
V	measured voltage from DC power supply, V
V_g	average volume of a departing bubble, m^3
x_m	mean vapor quality
z	axial coordinate for annular duct flow, mm

Greek symbols

ΔT	temperature difference, °C
ΔT_{sat}	wall superheat, $(T_w - T_{sat})$, °C
δ	gap size of annular duct, mm
μ_l	viscosity of liquid R-134a, N s/m^2
ρ_g, ρ_l	vapor and liquid densities of R-134a, kg/m^3
$\Delta\rho$	density difference, $\Delta\rho = \rho_l - \rho_g$, kg/m^3
σ	surface tension, N/m

where the heat transfer is dominated by the nucleate boiling. This is ascertained by the strong dependence of the boiling heat transfer coefficient on the heat flux and weak dependence on the mass flux and vapor quality [3–5,7,8,13,15–17]. Some studies show that both the nucleate boiling and convection are important in contributing the flow boiling heat transfer in small pipes [11,14]. Reducing the channel dimension was found to produce a negative effect on the boiling heat transfer [6,17], while the opposite trend is also noted [10,16,17]. The enhancing boiling heat transfer associated with the reduction in the channel dimension is attributed to three reasons. First, in the small channels the two phase flow is mainly in the confined bubble regime. The heat transfer in the confined bubble regime is shown to be very effective [6]. Secondly, the bubbles are squeezed and deformed to a larger extent in the small channels and the effects of the surface tension and friction shear stress are stronger. Besides, the cavities for nucleation on the channel walls can be more easily wetted [16]. Thirdly, the bubble departing frequency increases with the reduction in channel dimension, which in turn enhances the turbulence level in the flow [17].

To elucidate flow boiling heat transfer mechanism in small channels, the prevailing flow regimes need to be explored. Based on visualization of the flow and measurement of the heat transfer, three flow regimes have been suggested, namely, the isolated bubble, confined bubble and annular-slug flows [6,18]. However, some bubble behavior such as the bubble departure frequency, growth, sliding and departure size plays an important role in the flow boiling heat transfer. The bubble characteristics in the boiling flow have been examined by a number of research groups. For instance, Sheng and Palm [18] visualized the flow pattern and bubble shape for water in a single small glass tube ($D_h = 1.0$, 1.6, 2.0, 4.0 mm). The bubble departure diameter was noted to depend much on the mass flow rate. Recently, Lee et al. [19] and Li et al. [20] examined the bubble dynamics in a micro channel ($D_h = 41.3$ and 47.7 μm). The bubble departure radius was correlated by the modified form of the Levy equation.

The behavior of near-wall bubbles in subcooled flow boiling of water and R-134a in a vertical rectangular channel of conventional size ($D_h = 6.1$ mm) was investigated photographically by Bang et al. [21]. They described the coalescence of the bubbles and showed that the bubbles were smaller at a higher mass flux. The subcooled flow boiling and the associated bubble characteristics of R-134a in a horizontal annular channel

($D_h = 10.3$ mm) were examined by Yin et al. [22]. Results from their flow visualization indicated that the bubble generation was suppressed by raising the refrigerant mass flux and subcooling, and only the liquid subcooling exhibited a significant effect on the bubble size. Thorncroft et al. [23] experimentally investigated boiling of FC-87 in a vertical rectangular channel ($D_h = 12.7$ mm). Both the bubble growth and departure rates were noted to increase with the Jacob number, but the bubble departure diameter decreased with the mass flux. An experimental investigation of low pressure subcooled flow boiling inside a vertical concentric annulus ($D_h = 13.0$ mm) from Zeitoun and Shoukri [24] showed that the mean size and lift duration of the bubbles increased at decreasing liquid subcooling. Klausner et al. [25] developed a criterion for the bubble departure from the heated surface in the flow boiling of saturated refrigerant R-113 in a square duct ($D_h = 25.0$ mm). They found that the mean bubble departure diameter decreased with increasing mass flux and with decreasing heat flux. They also noted that before lifting off from the heated wall, the bubbles would slide a finite distance along the surface. Kocamustafaogullari and Ishii [26] developed a relation for active nucleation site density in pool boiling from the data available in the open literature. They also applied the correlation to the few available forced convection nucleate boiling data. The correlation was valid for the system pressure ranging from 1.0 to 198.0 bar.

In recent years, environmental concerns over the use of CFCs (chlorofluorocarbons) as the working fluids in refrigeration and air-conditioning systems have led to the development of alternative refrigerants. Among these alternatives, R-134a is used as a substitute for R-22. Moreover, considerable effort has been devoted to improving the design of more compact and efficient evaporators for the process and refrigeration industries. In spite of the extensive research on the flow boiling heat transfer, the bubble characteristics for the widely used refrigerant R-134a particularly in small channels remain largely unexplored. In this study, the saturated flow boiling of R-134a in an annular duct with a small gap between the inner and outer pipes is investigated by measuring the boiling heat transfer coefficient and by visualizing the bubble behavior. The effects of the imposed heat flux, gap size, mass flux and saturation temperature of R-134a on the boiling heat transfer characteristics will be examined in detail. Particularly, flow visualization is conducted here to examine some bubble characteristics associated with the flow boiling such as the mean bubble departure diameter and frequency from the heating surface to improve our understanding of the flow boiling processes in a narrow channel.

2. Experimental apparatus and procedures

The experimental system modified slightly from that used in the previous study [22] is employed here to investigate the saturated flow boiling heat transfer of R-134a in a narrow annular duct. It is schematically depicted in Fig. 1. The experimental apparatus consists of three main loops, namely, a refrigerant loop, a water–glycol

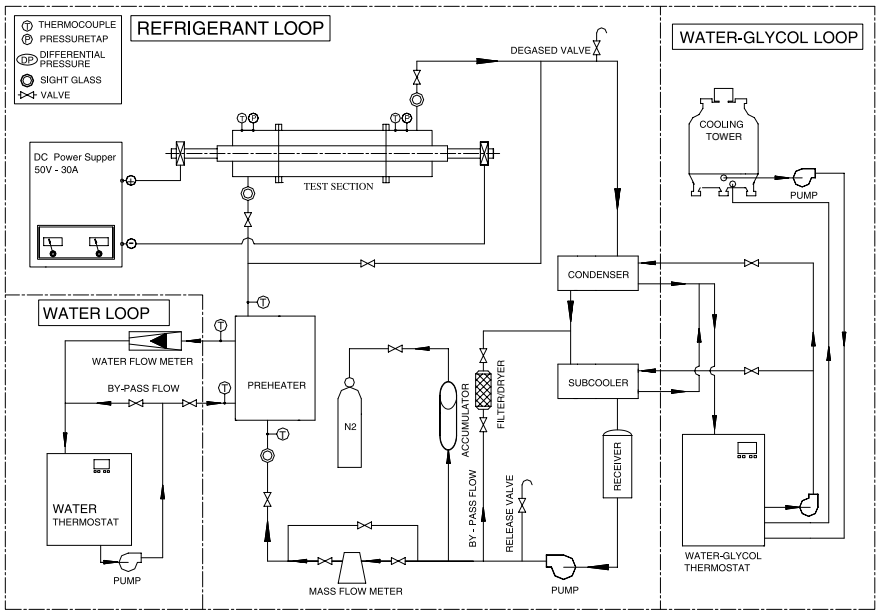

Fig. 1. Schematic of experimental system for the annular duct.

loop, and a hot-water loop. Refrigerant R-134a is circulated in the refrigerant loop. In order to control various test conditions of the refrigerants in the test section, we need to control the temperature and flow rate in the other two loops. The detailed description of the apparatus is available from our earlier study [22]. Here only the modified test section is described in detail.

As schematically shown in Fig. 2, the test section of the experimental apparatus is a horizontal annular duct with the outer pipe made of Pyrex glass to permit the visualization of boiling processes in the refrigerant flow. The glass pipe is 160 mm long with an inside diameter of 20.0 mm. Its wall is 4.0 mm thick. Both ends of the pipe are connected with copper tubes of the same size by means of flanges and are sealed by O-rings. The inner copper pipe has 16.0 or 18.0-mm nominal outside diameter with its wall being 1.5 or 2.5 mm thick and is 0.73 m long. Thus the gap of the annular duct is 2.0 or 1.0 mm ($D_h = 4.0$ or 2.0 mm). In order to insure the gap between the inner and outer pipes being uniform, we first measure the outside diameter of the inner pipe and the inside diameter of the glass pipe by digital calipers whose resolutions are 0.001 mm with the measurement accuracy of ± 0.01 mm. Then we photo the top and side view pictures of the annular duct and measure the average radial distance between the inside surface of the glass pipe to the outside surface of the inner tube. From the above procedures the duct gap is ascertained and its uncertainty is estimated to be 0.02 mm. An electric cartridge heater of 160 mm in length and 13.0 mm in diameter with a maximum power output of 800 W is inserted into the inner pipe. Furthermore, the pipe has an inactive heating zone of 10 mm long at each end and is insulated with Teflon blocks and thermally nonconducting epoxy to minimize heat loss from it. Thermal contact between the heater and the inner pipe is improved by coating a

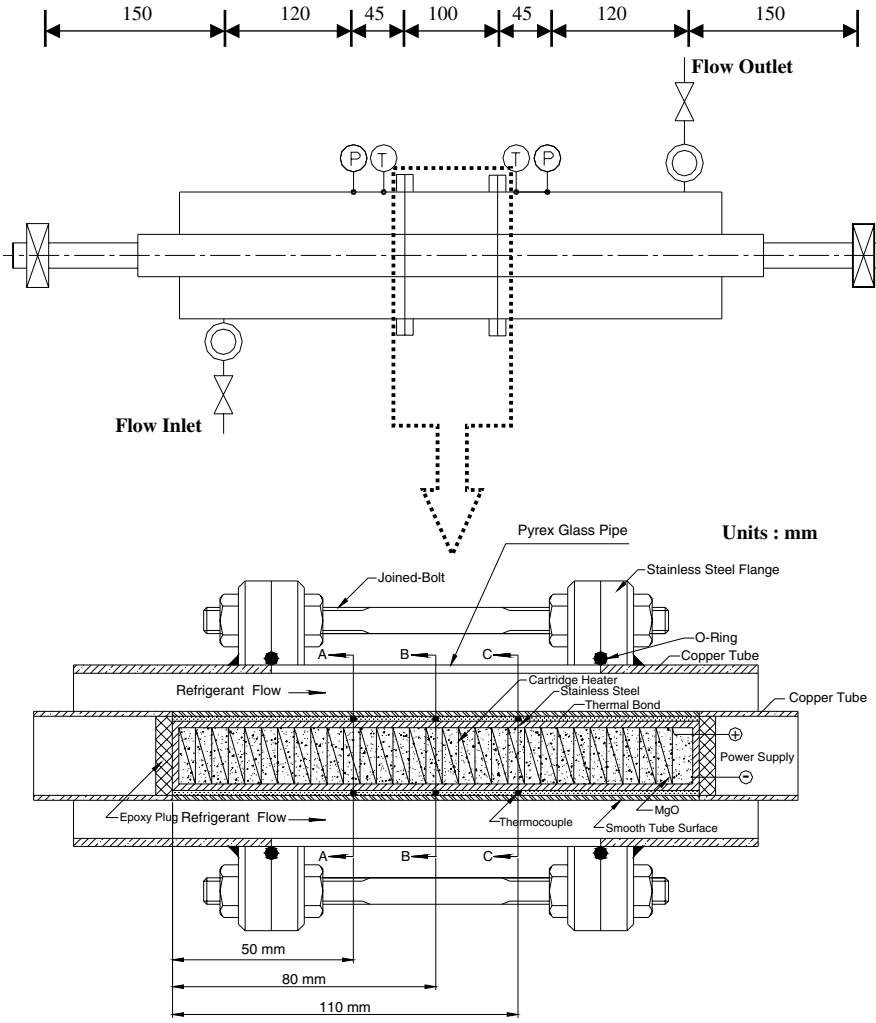

Fig. 2. The detailed arrangement of the test section for the annular duct.

thin layer of heat-sink compound on the heater surface before the installation of the heater. Then, 8 T-type calibrated thermocouples are electrically insulated by electrically nonconducting thermal bond before they are fixed on the inside surface of the inner pipe so that the voltage signals from the thermocouples are not interfered with the DC current passing through the cartridge heater. The thermocouples are positioned at three axial stations along the inner pipe. At each axial station, two to four thermocouples are placed at top, bottom, or two sides of the pipe circumference with 180° or 90° apart. The outside surface temperature T_w of the inner pipe is then derived from the measured inside surface temperature by taking into account the radial thermal conduction through the pipe wall.

The photographic apparatus established in the present study to record the bubble characteristics in the saturated flow boiling in the annular duct consists of a high speed digital video camera (Kodak Motion Corder Analyzer), a digital camera (Nikon D100), a three-dimensional positioning mechanism, and a personal computer. A Micro–Nikon 105 mm 1:2.8 lens is mounted on the camera. The high-speed motion analyzer can take photographs up to 10,000 frames/s. Here, a recording rate of 2,000 frames/s is adopted to obtain the images of the bubble ebullition processes in the flow boiling. The digital camera is used to take the overall pictures of the flow and the fastest shutter speed of the camera is 1/4,000 s. The positioning mechanism is used to hold the camera at the required accurate position. The data for the bubble characteristics are collected in the regions around the middle axial location ($z = 80$ mm). Note that the symbol z denotes the axial coordinate measuring from the inlet of the heated test section. After the experimental system reaches a statistically steady state, we start recording the boiling activity. The high-speed motion analyzer stores the images which are later downloaded to a personal computer. Then, the mean bubble departure diameter and frequency and active nucleation site density are calculated by viewing more than 500 frames for each case. In order to achieve the highest possible resolution and to eliminate errors in calibration, the camera lens is fixed at a constant focal length, resulting in a fixed viewing area. Typically, a total of over 150 bubble diameter measurements are used to construct the present data. The bubble departure frequency is measured by counting the total number of bubbles that emerge from the targeted heating surface during a period of 1 s.

Before a test is started, the temperature of refrigerant R-134a in the test section is compared with its saturation temperature corresponding to the measured saturation pressure and the allowable difference is kept below 0.3 K. Otherwise, the system is re-evacuated and then re-charged to remove the air existing in the refrigerant loop. In the test the liquid R-134a at the inlet of the test section is first maintained at the saturated temperature by adjusting the water–glycol temperature and flow rate. In addition, we adjust the thermostat temperature in the water loop to stabilize the refrigerant temperature at the test section inlet. Then, we regulate the refrigerant pressure at the test section inlet by adjusting the opening of the gate valve locating right after the exit of the test section. Meanwhile, by changing the current of the DC motor connecting to the refrigerant pump, the refrigerant flow rate can be varied. The imposed heat flux from the heater to the refrigerant is adjusted by varying the electric current delivered from the DC power supply. By measuring the current delivered to and voltage drop across the heater and by photographing the bubble activity, we can calculate the heat transfer rate to the refrigerant and obtain the bubble characteristics. All tests are run at statistically steady-state conditions. The whole system is considered to be at a statistically steady state when the time variations of the system pressure and imposed heat flux are respectively within ±1% and ±4%, and the time variations of the heated wall temperature are less than ±0.2 °C for a period of 100 min. Then all the data channels are scanned every 5 s for a period of 50 s.

3. Data reduction

The imposed heat flux for the refrigerant flow in the annular duct is calculated on the basis of the total power input and the total outside heat transfer area of the inner pipe A_s. The total power input is computed from the product of the measured voltage drop across the cartridge heater V and the electric current passing through it I. The imposed heat flux at the outside surface of the inner pipe is then evaluated from the relation

$$q = VI/A_s \tag{1}$$

Before the two-phase experiments, the total heat loss from the test section is evaluated by comparing the total power input from the power supply Q_s with the total heat transfer rate to the single-phase liquid refrigerant flow expressed as $G \cdot A_{cs} \cdot c_{pr} \cdot \Delta T$, where A_{cs} is the cross-sectional area of the annular duct and T is the difference in the refrigerant temperature at the exit and inlet of the test section. The relative heat loss from the test section is defined as

$$\varepsilon = (Q_s - G \cdot A_{cs} \cdot c_{pr} \cdot \Delta T)/Q_s \tag{2}$$

The results indicate that the heat loss from the test section is generally less than ±4% of the total power input. The outside surface temperature T_w of the inner heated pipe at each thermocouple location is deduced from the measured inside surface temperature of the pipe by accounting for the radial heat conduction in the pipe wall. In the two-phase test, the local saturated flow boiling heat transfer coefficient is defined as

Table 1
Summary of the uncertainty analysis

Parameter	Uncertainty
Annular pipe geometry	
Length, width and thickness (%)	±0.5%
Area (%)	±1.0%
Parameter measurement	
Temperature, T (°C)	±0.2
Temperature difference, ΔT (°C)	±0.3
System pressure, P (kPa)	±2
Mass flux of refrigerant, G (%)	±2
Saturated flow boiling heat transfer on small gap	
Imposed heat flux, q (%)	±4.5
Heat transfer coefficient, h_r (%)	±14.5

$$h_r = \frac{Q_n/A_s}{(T_w - T_{sat})} \tag{3}$$

Here Q_n is the net heat transfer rate to the refrigerant and is estimated as $Q_s\,(1-\varepsilon)$.

Uncertainties of the measured heat transfer coefficients are estimated according to the procedures proposed by Kline and McClintock [27] for the propagation of errors in physical measurement. The results from this uncertainty analysis are summarized in Table 1.

4. Results and discussion

In order to check the suitability of the experimental system for measuring the flow boiling heat transfer coefficients, the single-phase liquid R-134a heat transfer data are measured first and compared with the well-known traditional forced convection correlations proposed by Gnielinski [28] and Dittus–Boelter [29]. The results manifest that for $\delta = 2.0$ mm the present data can be well correlated with the above two correlations. But for the smaller gap of 1.0 mm only the Dittus–Boelter correlation can satisfactorily fit our data. Then, the present two-phase experiments are performed for the refrigerant mass flux G varying from 200 to 300 kg/m^{2}s, imposed heat flux q from 1 to 45 kW/m^2, and the system pressure P set at 414 kPa and 488 kPa (corresponding to the R-134a saturation temperature $T_{sat} = 10$ °C and 15 °C) for the gap of the duct $\delta = 1.0$ and 2.0 mm. The measured boiling heat transfer data are expressed in terms of the boiling curves and boiling heat transfer coefficient. Moreover, the side view flow photos taken at a small region around the middle axial station $z = 80$ mm are presented to illustrate the bubble characteristics in the boiling flow. Finally, empirical correlations are proposed to correlate the present data.

4.1. Saturated flow boiling curves

The effects of the experimental parameters including the refrigerant mass flux, gap size of the duct and refrigerant saturated temperature on the boiling curves measured at the middle axial location ($z = 80$ mm) of the narrow annular duct are illustrated in Fig. 3. The results in Fig. 3 indicate that at a low imposed heat flux the wall superheat of the heating surface is lower than that required for the onset of nucleate boiling (ONB) and no bubble nucleates from the heating surface. Hence heat transfer in the flow results completely from the single-phase liquid forced convection. As the imposed wall heat flux is raised gradually, the wall superheat increases correspondingly. At a certain wall superheat bubbles start

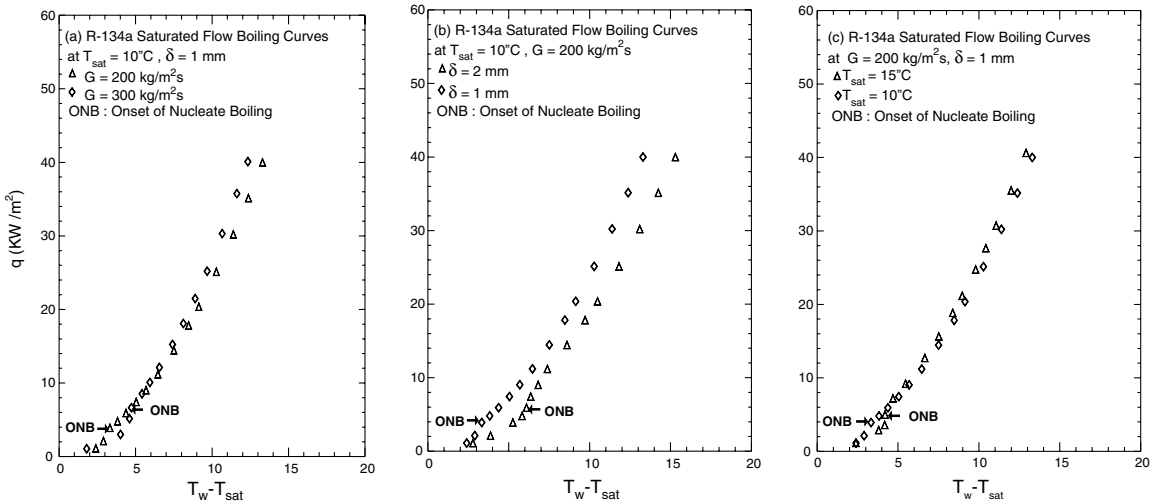

Fig. 3. Saturated flow boiling curves of R-134a: (a) for various refrigerant mass fluxes at $T_{sat} = 10$ °C and $\delta = 1$ mm, (b) for various gap sizes at $T_{sat} = 10$ °C and $G = 200$ kg/m^{2}s, and (c) for various saturated temperatures at $G = 200$ kg/m^{2}s and $\delta = 1$ mm.

to nucleate from the heating surface and we have ONB in the flow. Beyond the ONB there is a significant increase in the slope of the boiling curves, implying that a small rise in the wall superheat causes a large increase in the heat transfer rate from the wall to refrigerant. Note that at increasing refrigerant mass flux the boiling curve shifts slightly to the left (Fig. 3(a)), indicating that at a higher refrigerant mass flux the heat transfer in the saturated boiling is slightly better. This increase in the heat transfer rate with the mass flux is mainly due to the bubbles in the liquid refrigerant moving more vigorously and turbulently due to the higher refrigerant mass flux. The results also indicate that the required imposed heat flux to achieve ONB is influenced noticeably by the change in the mass flux. Specifically, the required imposed heat flux to achieve ONB is slightly higher for a higher mass flux. Then, it is further noted from Fig. 3(b) that the boiling curve shifts significantly to the left as the duct gap is reduced from 2.0 mm to 1.0 mm, indicating that the boiling heat transfer in smaller duct is substantially better. This also agrees with the findings of Qiu et al. [16] and Aritomi et al. [17]. It is also evident from the data given in Fig. 3(b) that the imposed heat flux needed to initiate boiling on the heated surface for the smaller duct is lower. Finally, the data shown in Fig. 3(c) suggest that the effects of the refrigerant saturation temperature on the boiling curves including the single-phase forced convection and nucleate boiling regimes are insignificant.

4.2. Saturated flow boiling heat transfer coefficient

The saturated flow boiling heat transfer coefficients of R-134a measured at the middle axial location ($z = 80$ mm) in the narrow annular duct affected by the three experimental parameters are shown in Fig. 4. The results indicate that at given G, δ and T_{sat} the saturated boiling heat transfer coefficient increases substantially with the boiling heat flux. For example, at $T_{sat} = 15$ °C, $\delta = 1.0$ mm and $G = 200$ kg/m^{2}s, the boiling heat transfer coefficient for $q = 40$ kW/m^2 is about 150% higher than that for $q = 5$ kW/m^2 (Fig. 4(a)). This large increase in h_r is ascribed to the higher active nucleation site density on the heating surface, higher bubble departure frequency and faster bubble growth for a higher imposed heat flux. We further noted from the data in Fig. 4(a) that the saturated boiling heat transfer coefficient rises noticeably with the refrigerant mass flux especially at a q exceeding 20 kW/m^2. The increase is larger for a high q. Then, the effects of the gap size of the duct on the saturated flow boiling heat transfer are shown in Fig. 4(b) and the data manifest that h_r increases significantly with a decrease in the channel gap. For instance, at $q = 40$ kW/m^2, $T_{sat} = 10$ °C and $G = 200$ kg/m^{2}s the saturated boiling heat transfer coefficient for $\delta = 1.0$ mm is about 20% higher than that for $\delta = 2.0$ mm. Since the shear stress of the forced liquid flow acting on the heated surface in the smaller channel becomes higher, the cavities on the heating surface can be more easily wetted and the bubbles are easier blown away from the heating surface causing a higher bubble departure frequency. These effects are thought to be the main reasons for the enhancement of nucleate boiling heat transfer when the channel size is reduced. Finally, the data shown in Fig. 4(c) suggest that the saturation temperature of the refrigerant exhibits negligible effects on the boiling heat transfer coefficient.

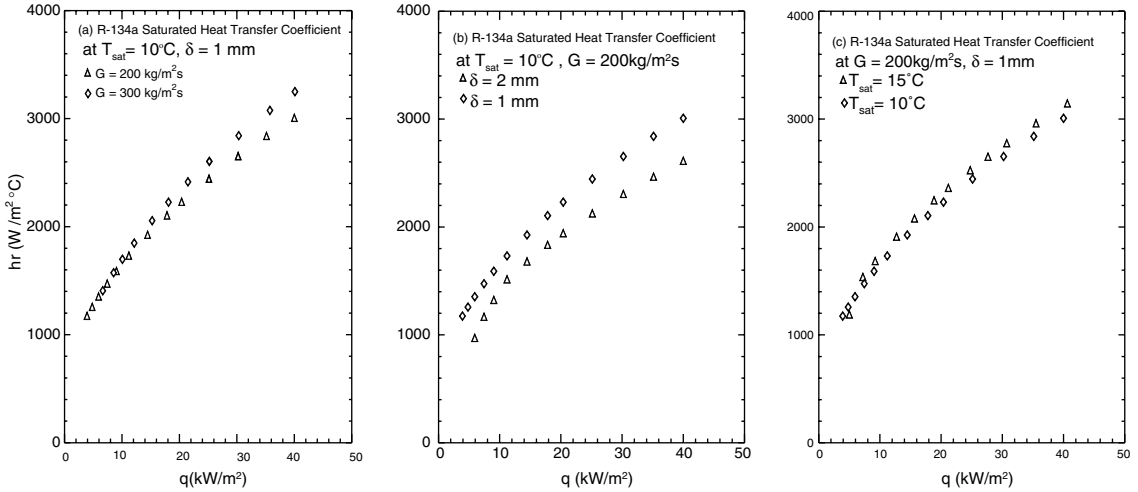

Fig. 4. Saturated flow boiling heat transfer coefficient of R-134a: (a) for various refrigerant mass fluxes at $T_{sat} = 10$ °C and $\delta = 1$ mm, (b) for various gap sizes at $T_{sat} = 10$°C and $G = 200$ kg/m^{2}s, and (c) for various saturated temperatures at $G = 200$ kg/m^{2}s and $\delta = 1$ mm.

4.3. Bubble characteristics in saturated flow boiling

To illustrate the bubble behavior in the duct, photos of the boiling flow of R-134a from the side and top view covering the entire narrow duct for the case with $G = 200\ \text{kg/m}^2\text{s}$, $T_{sat} = 15\ ^\circ\text{C}$, $\delta = 2.0\ \text{mm}$ and $q = 30\ \text{kW/m}^2$ are shown in Fig. 5. The results clearly indicate that in the relatively upstream region near the duct inlet a great number of bubbles already exist in the flow. Bubbles of varying size can be seen. Specifically, in the upper part of the duct larger bubbles dominate obviously due to the buoyancy effects. The photos of the boiling flow taken from the side view for the cases at different refrigerant mass fluxes, duct size and imposed heat fluxes in the small region around the middle axial location are shown in Fig. 6. First of all, it is noted from the photo taken from the smaller duct ($\delta = 1.0\ \text{mm}$) shown in Fig. 6(a) for the case at $T_{sat} = 15\ ^\circ\text{C}$ and $G = 200\ \text{kg/m}^2$ s at the imposed heat flux $q = 10\ \text{kW/m}^2$ that a large number of bubbles generated from the cavities in the heating surface tend to merge together to form big bubbles. As the bubbles get larger, they become distorted and elongated as they slide along the heating surface. When the imposed heat flux is raised slightly to $q = 15\ \text{kW/m}^2$ (Fig. 6(b)), the active bubble nucleation density increases and bubbles are observed to collide and coalesce more frequently. The coalescence bubbles rise faster than the tiny bubbles due to the larger buoyancy force associated with them. As the heat flux is raised over $20\ \text{kW/m}^2$ (Fig. 6(c)), coalescence of bubbles occurs irregularly. At even higher imposed heat flux for $q > 30\ \text{kW/m}^2$, the bubble departure frequency from the heating surface is very high so that it is difficult to clearly distinguish the individual bubbles leaving the surface. In general, the bubble departure frequency increases substantially with the imposed heat flux due to the fact that a rise in the imposed heat flux directly provides more energy to the cavities and more cavities on the heating surface can be activated. Besides, the bubble departure diameter increases slightly with the imposed heat flux due to the rise in the wall superheat.

Then, the corresponding photos taken from the larger duct with $\delta = 2.0\ \text{mm}$ shown in Fig. 6(d)–(f) indicate that in the larger duct less bubbles nucleate at the heated surface and hence less large bubbles result from the coalescence of the small bubbles especially at high heat flux. The bubble departure frequency is also lower and most bubbles are still distinguishable even at high heat flux. Finally, the bubble characteristics around the middle axial location affected by the refrigerant mass flux are examined

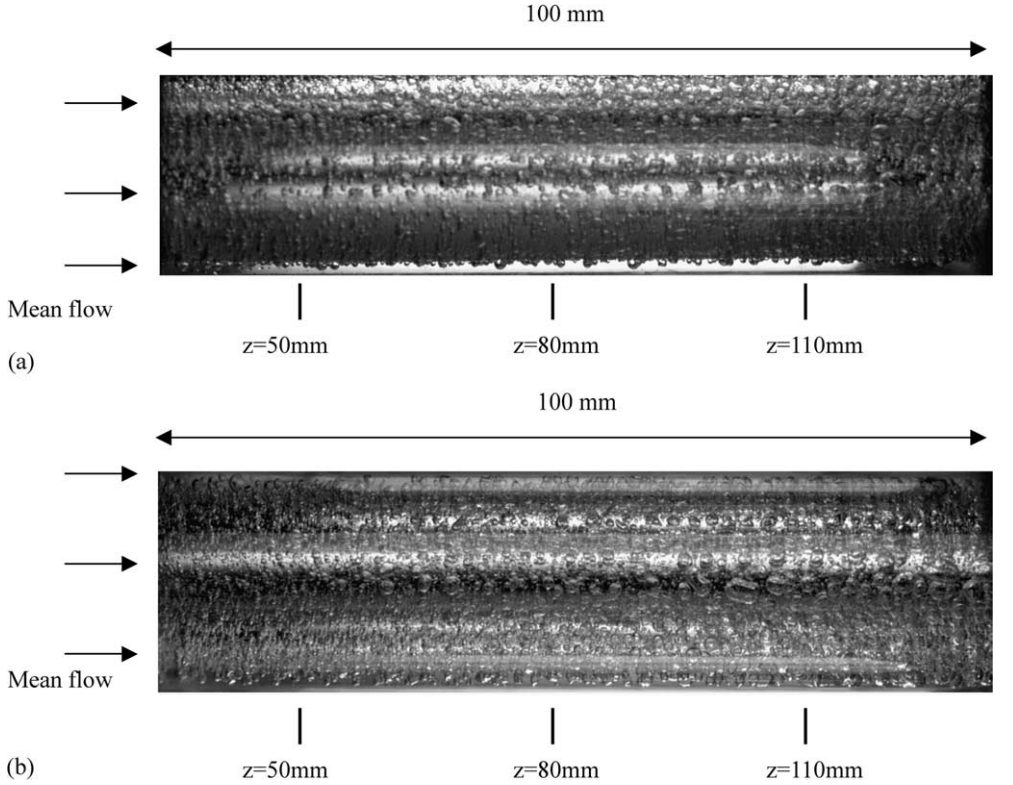

Fig. 5. Photos of boiling flow in the saturated flow boiling of R-134a in the entire duct at $G = 200\ \text{kg/m}^2\text{s}$, $T_{sat} = 15\ ^\circ\text{C}$, $\delta = 2\ \text{mm}$ and $q = 30\ \text{kW/m}^2$ from (a) side view and (b) top view.

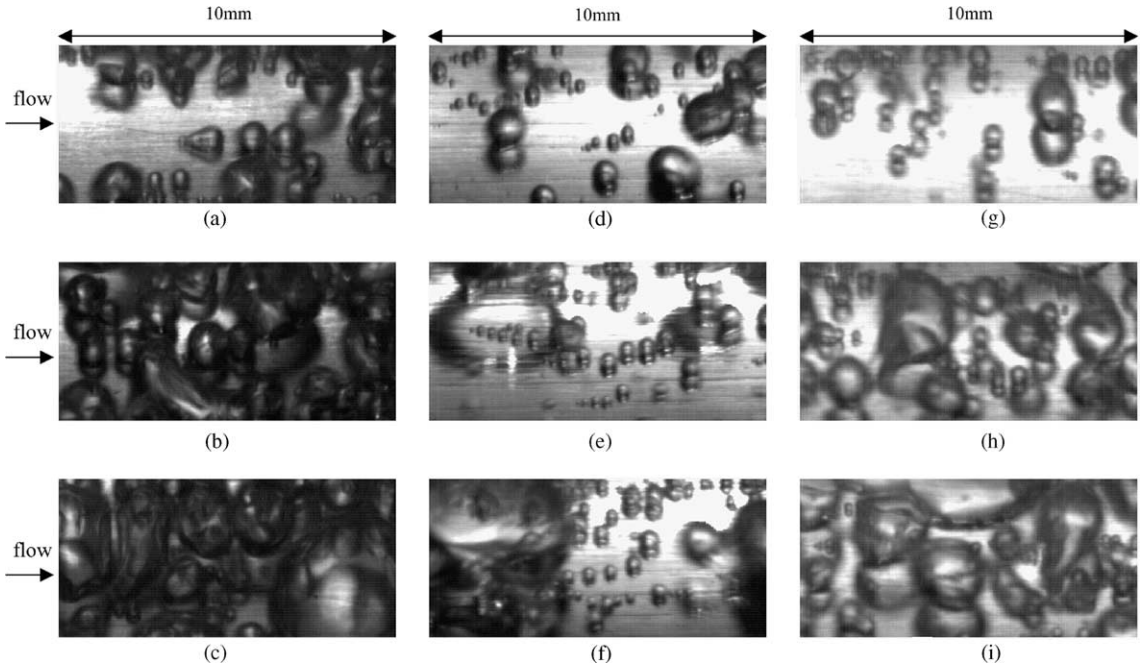

Fig. 6. Photos of bubbles in the saturated flow boiling of R-134a in a small region around middle axial location at $T_{sat} = 15$ °C for various imposed heat flux, mass fluxes and gap sizes: (a) $G = 200$ kg/m^{2}s, $q = 10$ kW/m^2, $\delta = 1.0$ mm; (b) $G = 200$ kg/m^{2}s, $q = 15$ kW/m^2, $\delta = 1.0$ mm; (c) $G = 200$ kg/m^{2}s, $q = 20$ kW/m^2, $\delta = 1.0$ mm; (d) $G = 200$ kg/m^{2}s, $q = 10$ kW/m^2, $\delta = 2.0$ mm; (e) $G = 200$ kg/m^{2}s, $q = 15$ kW/m^2, $\delta = 2.0$ mm; (f) $G = 200$ kg/m^{2}s, $q = 20$ kW/m^2, $\delta = 2.0$ mm; (g) $G = 300$ kg/m^{2}s, $q = 10$ kW/m^2, $\delta = 1.0$ mm; (h) $G = 300$ kg/m^{2}s, $q = 15$ kW/m^2, $\delta = 1.0$ mm; (i) $G = 300$ kg/m^{2}s, $q = 20$ kW/m^2, $\delta = 1.0$ mm.

by comparing the photos in Fig. 6(a)–(c) with Fig. 6(g)–(i). The results manifest that at a higher mass flux the liquid refrigerant flow moves at a higher speed, which tends to sweep the bubbles more quickly away from the heating surface. Thus, collision and coalescence of bubbles on the heating surface are also significant. Besides, the bubble departure frequency is higher and the bubbles are in violent agitating motion. However, at the higher G less bubble nucleation is activated on the heated wall and the active nucleation site density is lower. Note that at the low mass flux of 200 kg/m^{2}s the bubble coalescence is important and a number of big bubbles form in the duct.

To be more quantitative on the bubble characteristics, we estimate the average bubble departure diameter and frequency and the number density of the bubble nucleation on the heating surface from the images of the boiling flow stored in the video tapes. The results from this estimation are examined in the following. The effects of the three experimental parameters on the mean bubble departure diameter for the saturated flow boiling of R-134a at the middle axial location ($z = 80$ mm) in the annular duct are shown in Fig. 7. First, the variations of the average bubble departure diameter with the R-134a mass flux shown in Fig. 7(a) indicate that the average departing bubble is only slightly larger for a lower refrigerant mass flux. Then, the data given in Fig. 7(b) also suggest that the average bubble departing from the heated surface is slightly larger in the smaller duct. Finally, the results in Fig. 7(c) indicates that the average bubble departure diameter is somewhat smaller for a higher saturated temperature.

How the mean bubble departure frequency is affected by the three parameters for the saturated flow boiling of R-134a at the middle axial location ($z = 80$ mm) in the annular duct is illustrated in Fig. 8. First, the results in Fig. 8(a) indicate that the average bubble departure frequency is significantly higher for a higher refrigerant mass flux especially at a high imposed heat flux. For example, at $q = 20$ kw/m^2, $T_{sat} = 10$ °C and $\delta = 1.0$ mm, the average bubble departure frequency for $G = 300$ kg/m^{2}s is about 33% higher than that for $G = 200$ kg/m^{2}s. Then, the data in Fig. 8(b) and (c) manifest that the average bubble departure frequency is slightly higher in the smaller duct and at a high T_{sat}.

Finally, the effects of the experimental parameters on the number density of the active nucleation sites for ONB are shown in Fig. 9. The results given in Fig. 9(a) indicate that the average active nucleation site density is substantially higher for a smaller refrigerant mass flux especially at a high imposed heat flux. For example, at $q = 30$ kw/m^2, $T_{sat} = 15°$ and $\delta = 1.0$ mm, the average active nucleation site density for $G = 200$ kg/m^{2}s is about 25% higher than that for $G = 300$ kg/m^{2}s. We further note from Fig. 9(b) that the average active nucleation site

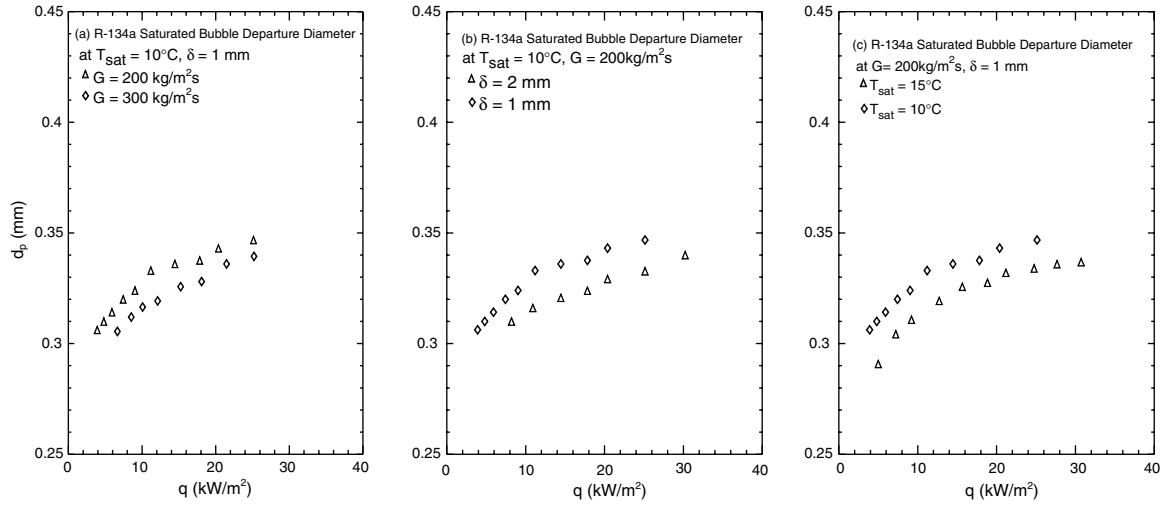

Fig. 7. Mean bubble departure diameter for saturated flow boiling of R-134a: (a) for various refrigerant mass fluxes at $T_{sat} = 10\ ^{\circ}C$ and $\delta = 10$ mm, (b) for various gap sizes at $T_{sat} = 10\ ^{\circ}C$ and $G = 200\ kg/m^2s$, and (c) for various saturated temperatures at $G = 200\ kg/m^2s$ and $\delta = 1$ mm.

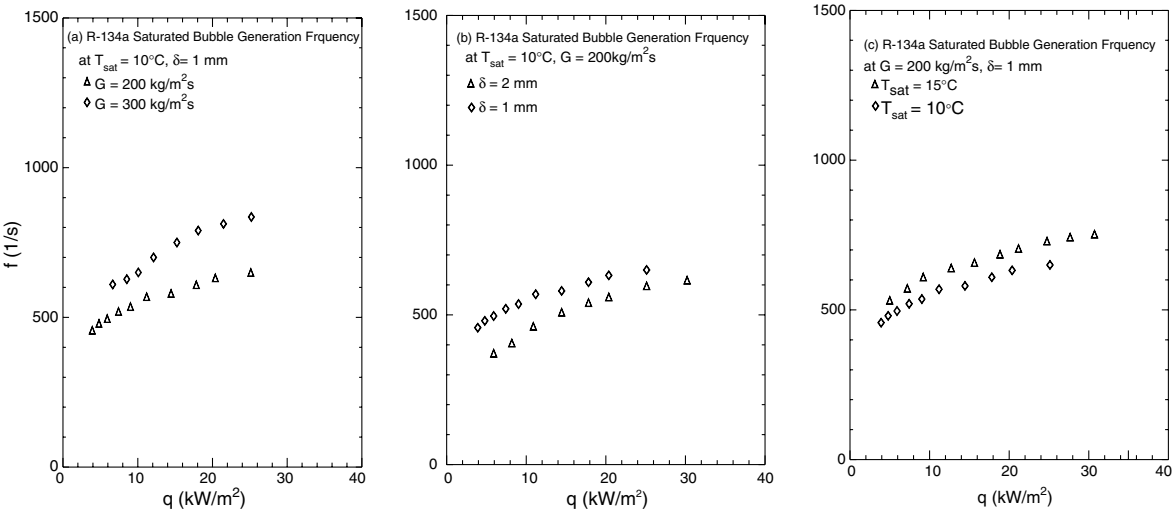

Fig. 8. Mean bubble departure frequency for saturated flow boiling of R-134a: (a) for various refrigerant mass fluxes at $T_{sat} = 10\ ^{\circ}C$ and $\delta = 1$ mm, (b) for various gap sizes at $T_{sat} = 10\ ^{\circ}C$ and $G = 200\ kg/m^2s$, and (c) for various saturated temperatures at $G = 200\ kg/m^2s$ and $\delta = 1$ mm.

density is only slightly affected by the duct size. The data shown in Fig. 9(c) suggest that the variations of the average active nucleation site density with T_{sat} are insignificant.

4.4. Correlation equations

According to the flow boiling mechanisms, the heat transfer in the flow boiling can be roughly considered as a combination of single-phase liquid convection heat transfer q_c and pool boiling nucleation heat transfer q_b. Thus the total heat flux input to the boiling flow q_t can be expressed as

$$q_t = q_b + q_c \tag{4}$$

Here q_b and q_c are respectively calculated from the relations

$$q_b = \rho_g \cdot V_g \cdot f \cdot N_{ac} \cdot i_{fg} \tag{5}$$

and

$$q_c = h_{1\phi} \cdot \Delta T_{sat} \tag{6}$$

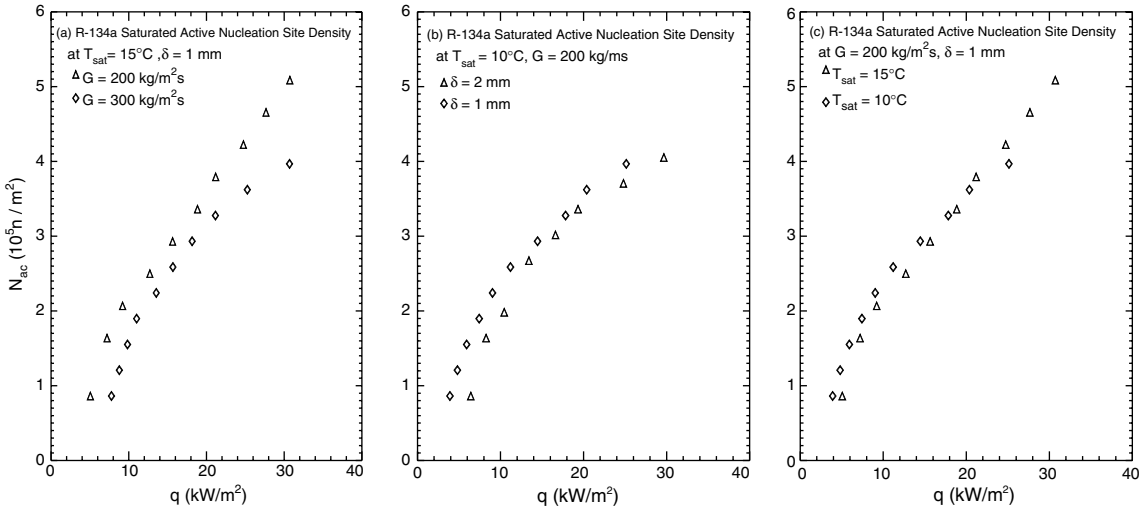

Fig. 9. Mean active nucleation site density for saturated flow boiling of R-134a: (a) for various refrigerant mass fluxes at $T_{sat} = 15$ °C and $\delta = 1$ mm, (b) for various gap sizes at $T_{sat} = 10$ °C and $G = 200$ kg/m^{2}s, and (c) for various saturated temperatures at $G = 200$ kg/m^{2}s and $\delta = 1$ mm.

Note that q_b expressed above in fact represents the latent heat carried away from the heating surface during the departure of bubbles from the surface. The single-phase forced convection heat transfer coefficient $h_{1\phi}$ is estimated from the correlation from Gnielinski [28] for the Nusselt number as

$$h_{1\phi} = Nu \cdot k_l / D_h \tag{7}$$

with

$$Nu = \frac{(f_f/2)(Re_l - 1000)Pr_l}{1.07 + 12.7\sqrt{f_f/2}(Pr_l^{2/3} - 1)} \tag{8}$$

Here the friction factor f_f is evaluated from the correlation

$$f_f = (1.58 \ln Re_l - 3.28b)^{-2} \tag{9}$$

Moreover, the Reynolds number of the liquid flow is defined as

$$Re_l = GD_h(1 - x_m)/\mu_l \tag{10}$$

In Eq. (5) ρ_g is the vapor density, V_g is the mean vapor volume of a departing bubble which is equal to $\frac{4\pi}{3}\left(\frac{d_p}{2}\right)^3$, f is the mean bubble departure frequency, N_{ac} is the average active nucleation site density, and i_{fg} is the enthalpy of vaporization. Because the present experimental Re_l ranges from 1000 to 6000, we use the Gnielinski correlation to estimate the single-phase convection heat transfer. At a higher imposed heat flux for $q > 30$ kW/m^2, it is difficult to distinguish the individual bubbles. Hence the above correlation does not apply to the data for $q > 30$ kW/m^2.

To enable the usage of the above correlation for the flow boiling heat transfer, the mean bubble size and departure frequency and the active nucleation density on the heating surface need to be correlated in advance. The average bubble departure diameter in the saturated flow boiling of R-134a in the narrow annular duct estimated from the present flow visualization can be correlated as

$$\frac{d_p}{\sqrt{\sigma/g \cdot \Delta\rho}} = 0.353\left(\frac{\rho_l}{\rho_g}\right)^{0.5} Re_l^{-0.2} \cdot Bo^{0.2} \cdot N_{conf}^{0.19} \tag{11}$$

Fig. 10 shows that almost all the present experimental data for d_p fall within ±25% of the above correlation and the mean absolute error is 10.8%. Besides, an empirical equation is proposed for the product of the mean bubble departure diameter and departure frequency as

$$\frac{f \cdot d_p}{\mu_l/(\rho_l D_h)} = 3.7 Re_l^{1.33} \cdot Pr_l^2 \cdot Bo^{0.725} \cdot N_{conf}^{0.59} \tag{12}$$

Note that more than 85% of the experimental data for $f \cdot d_p$ collected in this study can be correlated within ±25% by Eq. (12) and the mean absolute error is 14.4% (Fig. 11). Finally, we propose an empirical correlation for the average active nucleation site density in the saturated flow boiling of R-134a as

$$N_{ac} d_p^2 = -0.029 + 4.82 Bo^{0.409} Re_l^{-0.15} \tag{13}$$

Fig. 12 shows that the present experimental data fall within ±30% of the above correlation and the mean absolute error is 9.0%.

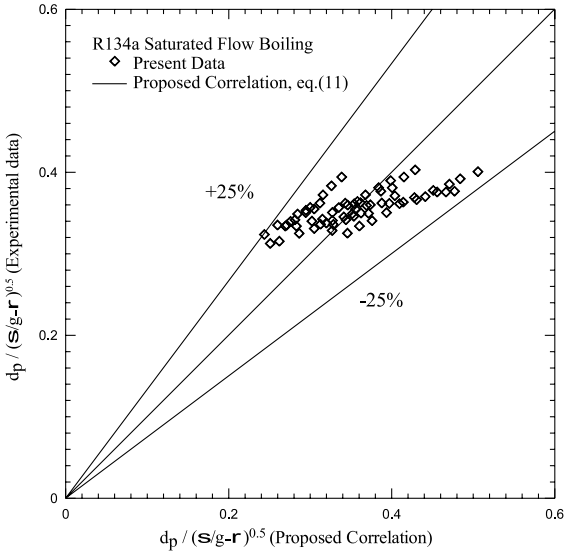

Fig. 10. Comparison of the measured data for mean bubble departure diameter in the saturated flow boiling of R-134a with the proposed correlation.

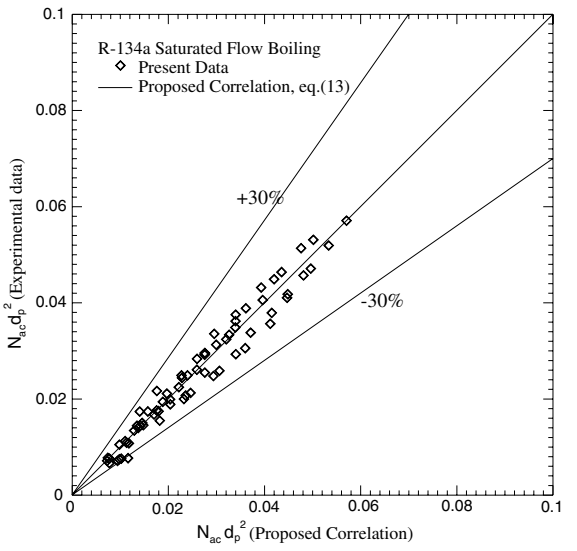

Fig. 12. Comparison of the measured data for mean active nucleation site density in the saturated flow boiling of R-134a with the proposed correlation.

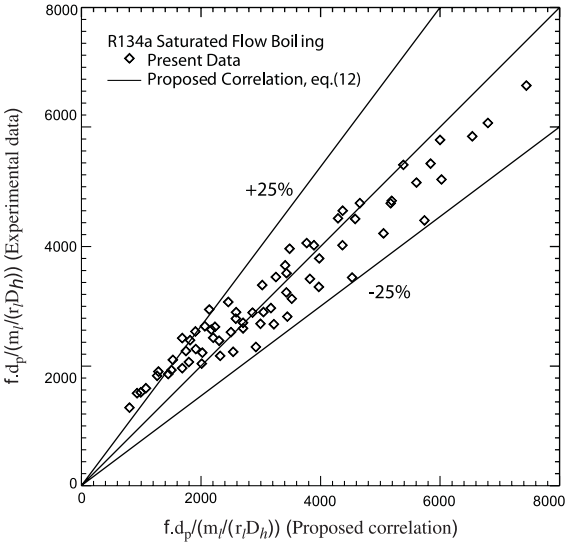

Fig. 11. Comparison of the measured data for mean bubble departure frequency in the saturated flow boiling of R-134a with the proposed correlation.

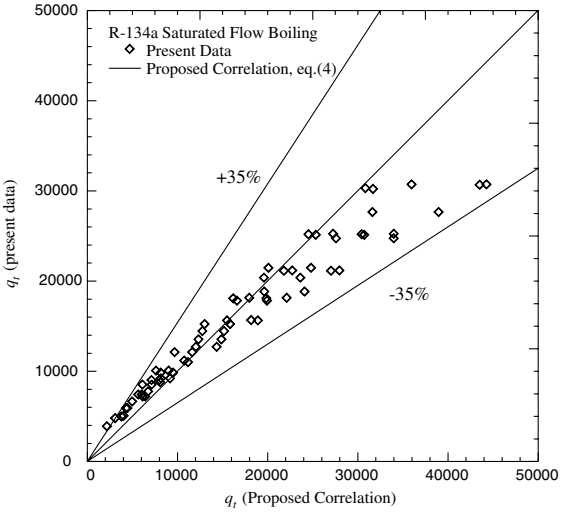

Fig. 13. Comparison of the measured data for heat transfer coefficient in the saturated flow boiling of R-134a with the proposed correlation.

When the correlations for d_p, f, and N_{ac} given in Eqs. (11)–(13) are combined with Eqs. (4)–(10) for q_t, more than 90% of the heat transfer data measured in the present study fall within ±35% of the correlation proposed here with the mean deviation of 15.7% (Fig. 13).

5. Concluding remarks

The measured heat transfer data for the saturated flow boiling of R-134a in the narrow annular duct have been presented here. Meanwhile, the bubble behavior in the boiling flow is examined. The effects of the imposed heat flux, refrigerant mass flux, system pressure and duct

size on the saturated flow boiling heat transfer coefficient and associated bubble characteristics have been investigated in detail. In addition, empirical equations to correlate the measured boiling heat transfer data, mean bubble departure diameter, bubble departure frequency and active nucleation site density are proposed. The major results obtained here can be summarized in the following.

(1) The saturated flow boiling heat transfer coefficient increases with a decrease in the gap size. Besides, raising the imposed heat flux can cause a significant increase in the boiling heat transfer coefficient. However, the effects of the refrigerant mass flux and saturated temperature on the boiling heat transfer coefficient are smaller but cannot be entirely neglected in the narrow duct examined here.
(2) The results from the flow visualization show that the mean diameter of the bubbles departing from the heating surface decreases slightly with increasing refrigerant mass flux. Besides, at a high imposed heat flux many bubbles generated from the cavities in the heating surface tend to merge together to form big bubbles. The mean bubble departure frequency increases with the increasing refrigerant mass flux and saturated temperature and with the decreasing duct size. Moreover, the active nucleation site density is much higher at a lower refrigerant mass flux particularly at a high imposed heat flux.
(3) The boiling heat transfer coefficient, mean bubble departure diameter, bubble departure frequency and active nucleation site density in the saturated flow boiling are correlated in terms of the relevant dimensionless groups.

Acknowledgement

The financial support of this study by the engineering division of National Science Council of Taiwan, R.O.C. through the contract NSC 92-2212-E-009-016 is greatly appreciated.

References

[1] S.S. Mehenendale, A.M. Jacobi, R.K. Shah, Fluid flow and heat transfer at micro- and meso-scale with application to heat exchanger design, Appl. Mech. Rev. 53 (2000) 175–193.
[2] B. Watel, Review of saturated flow boiling in small passages of compact heat exchangers, Int. J. Therm. Sci. 42 (2003) 107–140.
[3] W. Yu, D.M. France, M.W. Wambsganss, J.R. Hull, Two-phase pressure drop, boiling heat transfer, and critical heat flux to water in a small-diameter horizontal tube, Int. J. Multiphase Flow 28 (6) (2002) 927–941.
[4] Y. Fujita, Y. Yang, N. Fujita. Flow boiling heat transfer and pressure drop in uniformly heated small tubes, in: Proceedings of the Twelfth International Heat Transfer Conference, vol. 3, 2002, pp. 743–748.
[5] G.M. Lazarek, S.H. Black, Evaporative heat transfer, pressure drop and critical heat flux in a small vertical tube with R-113, Int. J. Heat Mass Transfer 25 (7) (1982) 945–960.
[6] P.A. Kew, K. Cornwell, Correlations for the prediction of boiling heat transfer in small-diameter channels, Appl. Therm. Eng. 17 (8–10) (1997) 705–715.
[7] T.N. Tran, M.W. Wambsganss, D.M. France, Small circular-and rectangular-channel boiling with two refrigerants, Int. J. Multiphase Flow 22 (3) (1996) 485–498.
[8] Z.Y. Bao, D.F. Fletcher, B.S. Haynes, Flow boiling heat transfer of Freon R11 and HCFC123 in narrow passages, Int. J. Heat Mass Transfer 43 (18) (2000) 3347–3358.
[9] G.R. Warrier, V.K. Dhir, L.A. Momoda, Heat transfer and pressure drop in narrow rectangular channels, Exp. Therm. Fluid Sci. 26 (1) (2002) 53–64.
[10] B. Sumith, F. Kaminaga, K. Matsumura, Saturated flow boiling of water in a vertical small diameter tube, Exp. Therm. Fluid Sci. 27 (7) (2003) 789–801.
[11] K. Moriyama, A. Inoue, H. Ohira, The thermohydraulic characteristics of two-phase flow in extremely narrow channels (The frictional pressure drop and heat transfer of boiling two-phase flow, Analytical Model), Heat Transfer—Japan. Res. 21 (8) (1992) 823–856.
[12] M. Kureta, T. Kobayashi, K. Mishima, H. Nishihara, Pressure drop and heat transfer for flow boiling of water in small-diameter tubes, JSME Int. J. Ser. B Fluids Thermal Eng. 41 (4) (1998) 871–879.
[13] T.N. Tran, M.W. Wambsganss, D.M. France, J.A. Jendrzejczyk, Boiling heat transfer in a small, horizontal, rectangular channel, Heat Transfer Atlanta AIChE Symp. Ser. 89 (295) (1993) 253–261.
[14] B.S. Haynes, D.F. Fletcher, Subcooled flow boiling heat transfer in narrow passages, Int. J. Heat Mass Transfer 46 (2003) 3673–3682.
[15] V.V. Kuznetsov, O.S. Kim, A.S. Shamirzaev, Flow boiling heat transfer in an annular channel with a small gap, Russ. J. Thermophys. 9 (4) (1999) 273–283.
[16] S. Qiu, M. Takahashi, G. Su, D. Jia, Experimental study on heat transfer of single-phase flow and boiling two-phase in vertical narrow annuli, in: Proceedings of 10th International Conference on Nuclear Engineering, vol. 3, 2002, pp. 319–324.
[17] M. Aritomi, T. Miyata, M. Horiguchi, A. Sudi, Thermo-hydraulics of boiling two-phase flow in high conversion light water reactors (thermo-hydraulics at low velocities), Int. J. Multiphase Flow 19 (1) (1993) 51–63.
[18] C.H. Sheng, B. Palm, The visualization of boiling in small diameter tubes, in: Proceedings of the International Conference on Heat Transfer and Transport Phenomena in Microscale, Banff, Canada, October 15–20, 2000, pp. 204–208.

[19] P.C. Lee, F.G. Tseng, C. Pan, Bubble dynamics in microchannels. Part I: single microchannel, Int. J. Heat Mass Transfer 47 (2004) 5575–5589.
[20] H.Y. Li, F.G. Tseng, C. Pan, Bubble dynamics in microchannels Part II: two parallel microchannels, Int. J. Heat Mass Transfer 47 (2004) 5591–5601.
[21] C. Bang, W.P. Baek, S.H. Chang, A digital photographic study on nucleate boiling in subcooled flow for water and refrigerant 134a fluids, in: Proceedings of 10th International Conference on Nuclear Engineering, Arlington, VA, April 14–18, 2002, vol. 3, pp. 155–162.
[22] C.P. Yin, Y.Y. Yan, T.F. Lin, B.C. Yang, Subcooled flow boiling heat transfer of R-134a and associated bubble characteristics in a horizontal annular channel, Int. J. Heat Mass Transfer 43 (2000) 1885–1896.
[23] G.E. Thorncroft, J.F. Klausner, R. Mei, An experimental investigation of bubble growth and detachment in vertical upflow and downflow boiling, Int. J. Heat and Mass Transfer 41 (23) (1998) 3857–3871.
[24] O. Zeitoun, M. Shoukri, Bubble behavior and mean diameter in subcooled flow boiling, ASME J. Heat Transfer 118 (1996) 110–116.
[25] J.F. Klausner, R. Mei, D.M. Bernhard, L.Z. Zeng, Vapor bubble departure in forced convection boiling, Int. J. Heat Mass Transfer 36 (3) (1993) 651–662.
[26] G. Kocamustafaogullari, M. Ishii, Interfacial area and nucleation site density in boiling systems, Int. J. Heat Mass Transfer 26 (9) (1983) 1377–1387.
[27] S.J. Kline, F.A. McClintock, Describing uncertainties in single-sample experiments, Mech. Eng. 75 (1) (1953) 3–12.
[28] V. Gnielinski, New equations for heat and mass transfer in turbulent pipe and channel flow, Int. Chem. Eng. 16 (2) (1976) 359–368.
[29] F.W. Dittus, L.M.K. BoelterHeat Transfer in Automobile Radiator of the Tube Type, vol. 2, University of California Publication in Engineering, Berkley, 1930, p. 250.